Research Article
Effects of Surfactants on the Performance of CeO$_2$ Humidity Sensor

Chunjie Wang,[1] Aihua Zhang,[1] and Hamid Reza Karimi[2]

[1] *College of Engineering, Bohai University, Jinzhou 121013, China*
[2] *Department of Engineering, Faculty of Engineering and Science, University of Agder, 4898 Grimstad, Norway*

Correspondence should be addressed to Chunjie Wang; cjwang@foxmail.com

Nanosized CeO$_2$ powders were synthesized via hydrothermal method with different types of surfactants (polyethylene glycol (PEG), cetyltrimethylammonium bromide (CTAB), and sodium dodecylbenzenesulfonate (SDBS)). X-ray diffraction, Raman spectroscopy, and transmission electron microscopy were utilized to characterize the phase structures and morphologies of the products. The sample with CTAB as surfactant (CeO$_2$-C) has the largest specific surface area and the smallest particle size among these three samples. The humidity sensor fabricated by CeO$_2$-C shows higher performance than those used CeO$_2$-P and CeO$_2$-S. The impedance of the CeO$_2$-C sensor decreases by about five orders of magnitude with relative humidity (RH) changing from 15.7 to 95%. The response and recovery time are 7 and 7 s, respectively. These results indicate that the performance of CeO$_2$ humidity sensors can be improved effectively by the addition of cationic surfactant.

1. Introduction

In recent decades, humidity sensors have received intense interests for their wide applications in environment protection, agriculture, and industrial production driven by the recognized importance of vapor concentration [1–4]. The materials for humidity sensors are generally including organic polymer films and porous ceramic films [5, 6]. The main disadvantages of humidity sensors based on the former are the weak mechanical strength, poor physical and chemical stability, and low operation temperature. For the latter, the dull response and recovery time are the main challenge. In recent years, many efforts have been carried out to explore the materials of humidity sensors, such as SnO$_2$, TiO$_2$, ZnO, and BaTiO$_3$ [7–10]. As one of the candidate materials of sensor, cerium oxide shows large diffusion coefficient for oxygen vacancy and good corrosion resistance to corrosive gases (Cl$_2$, SO$_2$ and NO) [11]. Based on the merit mentioned above, CeO$_2$ becomes heatedly discussed topic in recent years.

In the past few years, several methods have been proposed to prepare fine nanopowders. Hydrothermal method is considered as one of the most promising techniques for the room temperature manufacture of nanopowders, which can be attributed to the advantages related to the homogeneous nucleation processes and fine grain size. However, due to the high surface energy, nanoparticles are easy to coagulate and difficult to disperse. It is well known that serious agglomeration has an adverse effect on the properties of sensors during the filming process. Kinds of surfactants have been introduced to improve the performance of the materials [12, 13]. Nevertheless, to the best of our knowledge, the systematic investigation of the effects of different types of surfactants (nonionic, cationic, and anionic) on the performance of CeO$_2$ as humidity sensor has not been reported. To improve the performance of sensing materials, it is essential to make insight into the characteristics with different surfactants.

In this paper, three different kinds of surfactants, that is, PEG (nonionic), CTAB (cationic), and SDBS (anionic), were used as surfactants to prepare CeO$_2$ nanopowders via hydrothermal process, and the effects of surfactants on the structures and the humidity sensing properties of the corresponding sensors were investigated in detail. The main purpose of this study is to clarify the influence of surfactants on the performance of the CeO$_2$ humidity sensor.

2. Experimental Details

Based on the conventional hydrothermal method, CeO_2 nanopowders with different surfactants were synthesized as follows: $Ce(NO_3)_3 \cdot 6H_2O$ (99.99%, Chenghai Chemical of Guangdong), CTAB, PEG, and SDBS (Shanghai Chemicals Ltd.) were used as starting material and surfactants. A certain amount of surfactants (2 wt.%) was added into 50 mL of $Ce(NO_3)_3$ solution (0.1 M) under magnetic stirring. The pH value of the solution was adjusted to 7 by adding sodium hydroxide solution (2 M). Then, CeO_2 nanopowders were obtained by hydrothermal treatment for the mixed solution at 180°C for 24 h in a Teflon autoclave. The precipitates were filtered and washed with distilled water and ethanol for several times and dried at 70°C for 12 h. The same procedure was followed for the preparation of CeO_2 nanocrystalline powders by using CTAB, PEG, and SDBS as surfactants, respectively. In this paper, three produced CeO_2 nanopowders were designated as CeO_2-P, CeO_2-C, and CeO_2-S, respectively.

The crystalline phases of CeO_2 nanocrystalline powders were examined by means of powder X-ray diffraction (XRD, Bruker D8 Focus powder X-ray diffractometer) using Cu Kα radiation ($\lambda = 1.5406$ Å) with a scanning rate of 5°·min^{-1}. The operation current and voltage were maintained at 40 mA and 40 kV, respectively. The lattice parameters were calculated based on these XRD patterns. The average particle size of nanopowders (D) was determined by Scherrer's equation [14]:

$$D = \lambda \frac{K}{\beta \cos \theta}, \tag{1}$$

where λ is the wavelength of the X-ray radiation, θ is the diffraction angle, K is a constant (0.89), and β is the corrected full-width half maximum (FWHM). The Gaussian-Gaussian relationship [14] was also used for the instrument correction:

$$\beta^2 = B^2 - b^2, \tag{2}$$

where FWHM of the sample and the standard width of reference silicon sample are represented by B and b, respectively.

FT-Raman spectra were recorded on a Thermo Nicolet 960 instrument with an excitation wavelength of 1064 nm, and the measured wave number range is from 100 to 900 cm^{-1}. The specific surface area (S_{BET}) was determined by applying Brunauer-Emmet-Teller (BET) equation [15, 16] with a Micromeritics ASAP2020 instrument. The microstructures, morphologies, and particle sizes of the three samples were examined by a Philips TF-F20 electron transmission microscope.

In order to fabricate the humidity sensors, the CeO_2 nanopowders were dispersed in ethanol by magnetic stirring (30 min). The mixed solution was dropped onto a ceramic substrate (6 cm × 3 cm, 0.5 cm in thick) with a pair of Ag-Pd interdigital electrodes to form a CeO_2 film with a thickness of 10 μm. Furthermore, the humidity sensors were annealed at 180°C for 1 h. The characteristic curves of humidity sensitivity were measured on a ZL-5 model LCR analyzer (Shanghai, China). In our study, the voltage was fixed at 1 V. The humidity environments were obtained by
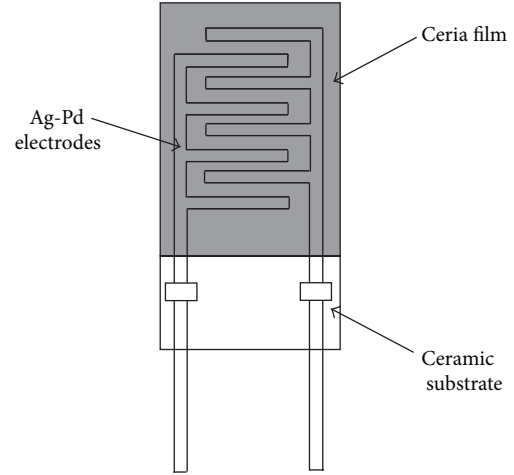

Figure 1: Schematic diagram of the sensor structure.

using $MgCl_2$, $Mg(NO_3)_3$, NaCl, KCl, and KNO_3 saturated salt solutions, and the corresponding RH values were 33, 54, 75, 85, and 95%, respectively. The humidity of laboratory atmosphere was 15.7% RH controlled by an automatic drier. Figure 1 shows the schematic diagram of the sensor structure.

3. Results and Discussion

The crystal structures of the as-prepared products were examined by XRD, and the corresponding results are shown in Figure 2(a). The XRD patterns of three samples show a face-centered cubic structure of ceria [JCPDS 43-1002]. As shown in Figure 2(a), the peaks at round $2\theta = 29.8°$, $34.6°$, $49.6°$, $59.2°$, and $72.8°$ are assigned to the (111), (200), (220), (311), and (400) reflections, respectively. It is worth noting that the diffraction peak width of CeO_2-C is wider than those of CeO_2-P and CeO_2-S, implying that the grain size of CeO_2-C is the smallest among the three samples. In addition, the composition of the as-synthesized products was further examined using an energy dispersive X-ray spectrometer (EDS). Figure 2(b) shows the EDS spectrum of CeO_2-C, and only three elements (Ce, O and Si) can be identified in this spectrum. The chemical composition of CeO_2-C is very close to the stoichiometric composition of CeO_2. The presence of Si in the spectrum can be attributed to the Si substrate. Furthermore, the average crystallite sizes, specific surface areas, and lattice parameters of three samples were also investigated, as shown in Table 1. The crystal size was calculated by Scherrer's equation as mentioned in experimental section. For CeO_2-C, the average crystallite size is 17.34 nm, while those of CeO_2-P and CeO_2-S are 19.27 and 21.42 nm, respectively. The lattice parameters are calculated from the XRD patterns using software JADE 5.0, and the determined value of each lattice parameter is the average value of 5 samples. For CeO_2-C, the calculated value is 5.3945 ± 0.0002 nm, which is higher than those of CeO_2-P (5.3726 ± 0.0002 nm) and CeO_2-S (5.3544 ± 0.0003 nm). In the case of specific surface area, the values for CeO_2-C, CeO_2-P, and CeO_2-S are 143.45, 116.87, and 99.36 m^2·g^{-1}, respectively. For nanomaterials, the crystal

(a)

(b)
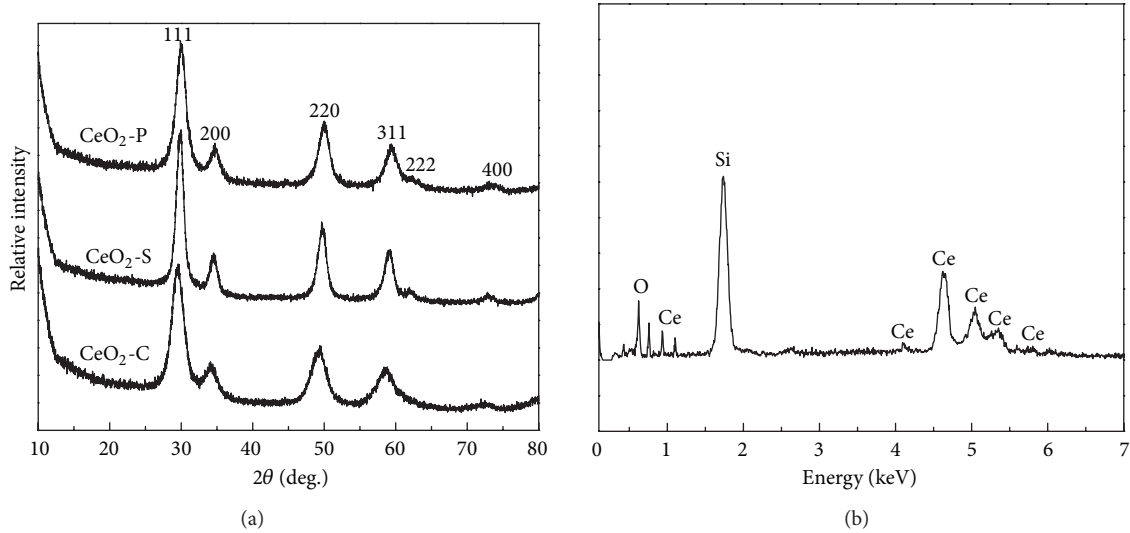
FIGURE 2: XRD patterns of the as-synthesized samples (a) and EDS pattern of as-prepared CeO_2-C (b).

TABLE 1: The specific surface areas, crystalline sizes, and lattice parameters for three samples.

Samples	Specific surface area ($m^2 \cdot g^{-1}$)	Crystallite size (nm)	Lattice parameter (nm)
CeO_2-P	116.87	19.27	5.3726 ± 0.0002
CeO_2-C	143.45	17.34	5.3945 ± 0.0002
CeO_2-S	99.36	21.42	5.3544 ± 0.0003

FIGURE 3: Raman spectra of CeO_2-P, CeO_2-C, and CeO_2-S nanopowders.

size is closely related to the specific surface area. The smaller the crystal size is, the higher the specific surface area will be. From the data of average particle sizes mentioned above, the specific surface areas of these three samples should decrease in the following order: CeO_2-C > CeO_2-P > CeO_2-S. This trend is coincident with the measurement values in this study. As is well known, the structure, surface area, crystallite size could be influenced by the different elective adsorption processes and the interactions between the surfactant and inorganic precursor molecules during the nucleation process. However, the related mechanism is more complicated and needs to be further investigated.

In order to confirm the phase structure, the as-prepared samples were further examined by Raman spectroscopy in the wave number range of $100\sim900\,cm^{-1}$, as represented in Figure 3. Careful investigation of the spectra revealed a detailed structure of cubic type. It can be noted from Figure 3 that the main band at $469\,cm^{-1}$ can be attributed to the F_{2g} vibration mode from the space group *Fm3m* of cubic structure [17, 18]. This further confirms that the structures of three samples are cubic phase as mentioned in XRD analysis. Moreover, it can be seen that a small shoulder appeared at about $600\,cm^{-1}$, which should be assigned as the longitudinal optical mode [19]. In the present case, the intensity of the band at $469\,cm^{-1}$ for CeO_2-C is higher than those for the other two samples.

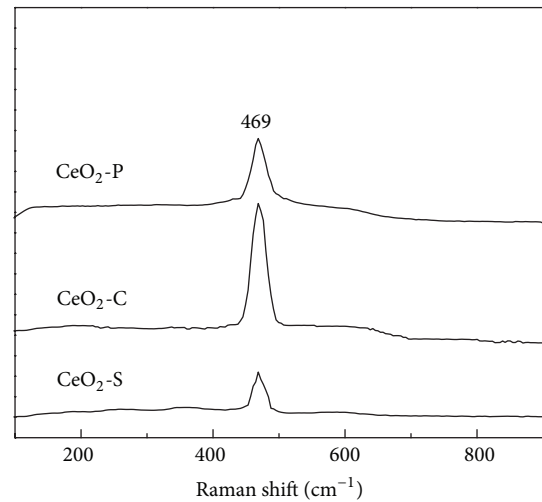The morphologies and particle sizes of three samples were investigated by TEM, as shown in Figure 4. All of these three samples show a monodispersed square shape, and the particle size of CeO_2-C is more uniform than those of CeO_2-P and CeO_2-S. The average particle sizes of three samples were also calculated, and the determined particle size was the averaged value of 40 particles selected randomly in the figure. For CeO_2-P, CeO_2-C, and CeO_2-S, the calculated average particle sizes are 19.76, 17.88, and 21.77 nm, respectively. These results are consistent with earlier data in XRD analysis mentioned above.

Figure 5 shows the characteristics of resistance versus relative humidity (RH) of three samples with different surfactants measured at room temperature in the relative humidity range from 15.7 to 95%. In this study, the surfactants obviously have an important influence on the humidity dependence of
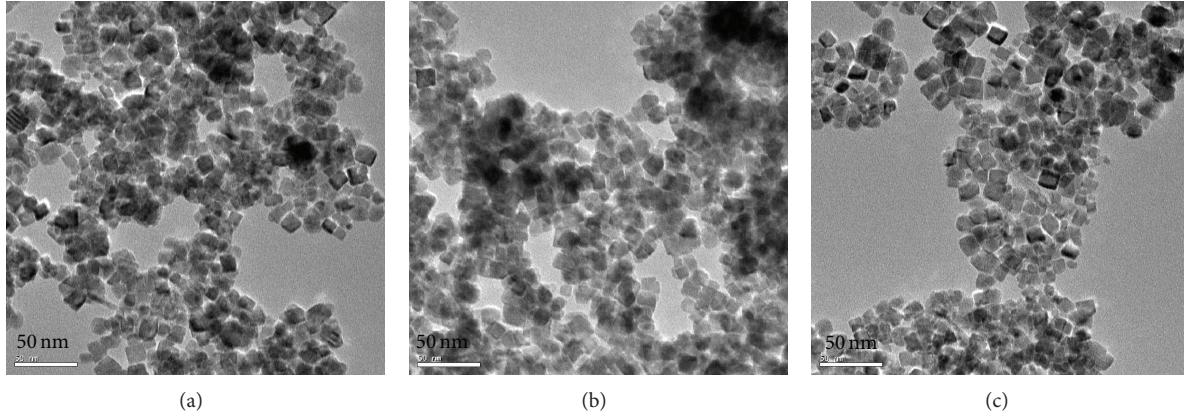
(a)   (b)   (c)

FIGURE 4: TEM image of three as-prepared samples: (a) CeO$_2$-P, (b) CeO$_2$-C, and (c) CeO$_2$-S.
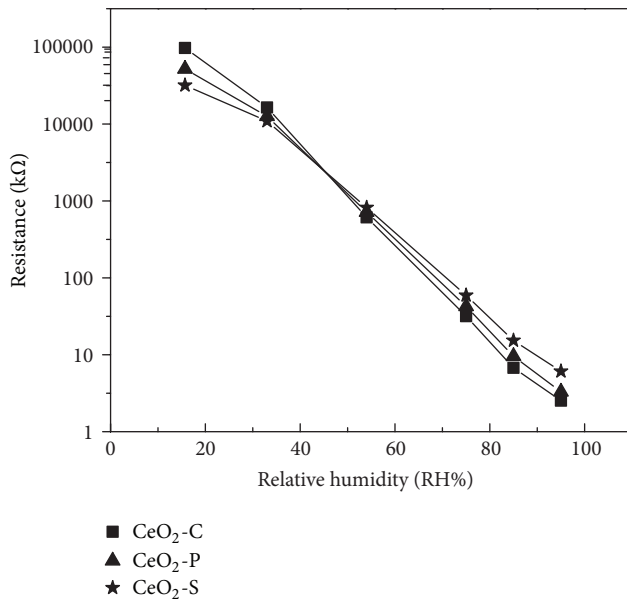
■ CeO$_2$-C
▲ CeO$_2$-P
★ CeO$_2$-S

FIGURE 5: Resistance versus RH plots of CeO$_2$ sensor with different surfactants.

FIGURE 6: Response and recovery characteristics of CeO$_2$ sensors with different surfactants.

the impedance of sensors. As a comparison among these three samples, the decrease of impedance for CeO$_2$-C is greater than those for CeO$_2$-P and CeO$_2$-S. The high humidity sensitivity and the best linearity of the impedance versus RH curve appeared in CeO$_2$-C. By contrast, in the case of CeO$_2$-S, the situation is just the reverse compared with CeO$_2$-C. For CeO$_2$-C, moreover, the impedance change is more than five orders of magnitude.

Response and recovery behaviors are the significant characteristics for estimating the performance of humidity sensor. Response time for adsorption process and recovery time in the case of desorption are defined as the time taken by the sensor to achieve 90% variable quantity. Based on the results mentioned above, the response and recovery behaviors of three samples were investigated. The sensor is transferred from initial atmosphere (33% RH) to target atmosphere (95% RH) and transferred back to investigate
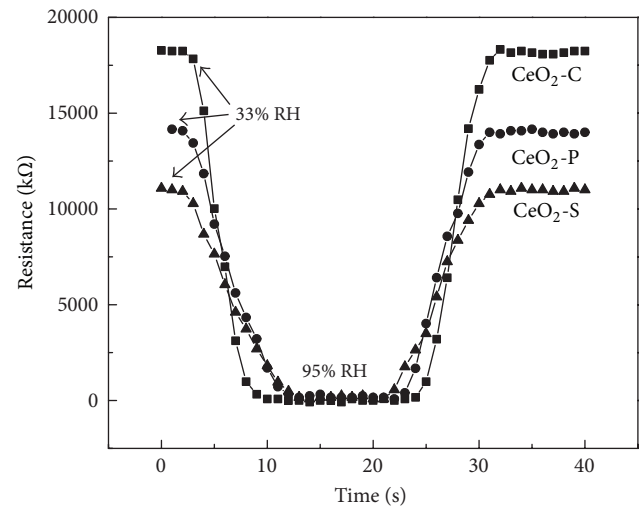
the response and recovery time, respectively. As shown in Figure 6, the humidity sensor fabricated from CeO$_2$-C shows rapid response-recovery characteristics. The response time (humidification from 33 to 95% RH) and the recovery time (desiccation from 95 to 33% RH) are about 7 s and 7 s, respectively. In the cases of CeO$_2$-P and CeO$_2$-S, however, the corresponding response and recovery time are 10, 9 s and 12, 11 s, respectively. Such facts indicate that the cationic surfactant (CTAB) has a significant effect on improving the performance of CeO$_2$ humidity sensors.

It is well known that the humidity sensing is closely related to the adsorption process of water molecules on the surface of the nanoparticles. The number of water molecules adsorbed on the powders has an important effect on electrical response. In the case of low humidity, only a few water molecules can be adsorbed on the surface of the film by the chemisorption mechanism [20–22]. The discontinuous layer of water molecules on the surface of the film leads to the difficulty of electrolytic conduction. According to

Schaub et al. studies [23–25], the high local charge density and a strong electrostatic field result from the tip, defects, and contracts of the powders can promote water dissociation to provide charge carriers. For high humidity, however, more and more water layers can be formed on the surface of nanoparticles by physisorption mechanism. As the dominant charged carriers, H^+ decomposed from water molecules can further decrease the impedance. On the other hand, in our study, the nanosized grains and the high specific surface area also play an important role in the sensor performance. The nanoscale grain size shows much more grain boundaries which produce large amount of active sites available for water molecules to react. Also, the CeO_2-C nanoparticles have the largest specific surface area among the three samples. The large surface of the nanomaterials makes the water molecules absorbed on the surface of the sensor easily, which can improve the response and recovery characteristics. So the response and recovery time of CeO_2-C are faster compared with CeO_2-P and CeO_2-S. In accordance with the results of the study, a conclusion can be drawn that cationic surfactant (CTAB) has a significant effect on improving the sensibility of CeO_2 humidity sensor compared with nonionic surfactant (PEG) and anionic surfactant (SDBS).

4. Conclusions

CeO_2 nanoparticles with three different types of surfactants were synthesized via hydrothermal method. The CeO_2-C has the largest specific surface area and the smallest particle size. The performances of the corresponding sensors were also investigated in detail. By comparison, cationic surfactant (CTAB) has a significant effect on improving the performance of humidity sensor compared with the other two surfactants (nonionic (PEG) and anionic (SDBS)). The CeO_2-C humidity sensor shows a high sensitivity, fast response (7 s), and rapid recovery (7 s) characteristics in the humidity range of 33~95% RH, while the response and recovery time for CeO_2-P and CeO_2-S are 10, 9 s and 12, 11 s, respectively.

Conflict of Interests

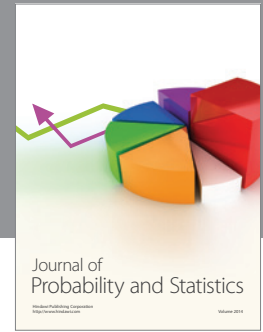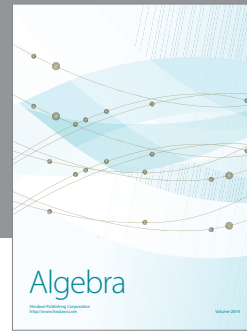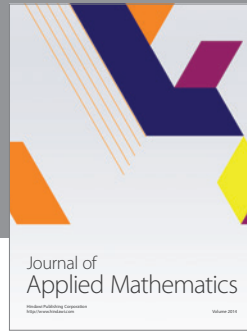The authors declare that there is no conflict of interests regarding the publication of this paper.

Acknowledgment

References

[1] S. Zampolli, I. Elmi, J. Stürmann, S. Nicoletti, L. Dori, and G. C. Cardinali, "Selectivity enhancement of metal oxide gas sensors using a micromachined gas chromatographic column," *Sensors and Actuators B*, vol. 105, no. 2, pp. 400–406, 2005.

[2] S. Ehrmann, J. Jüngst, J. Goschnick, and D. Everhard, "Application of a gas sensor microarray to human breath analysis," *Sensors and Actuators B*, vol. 65, no. 1, pp. 247–249, 2000.

[3] S. Yin, G. Wang, and H. Karimi, "Data-driven design of robust fault detection system for wind turbines," *Mechatronics*, 2013.

[4] S. Yin, H. Luo, and S. Ding, "Real-time implementation of fault-tolerant control systems with performance optimization," *IEEE Transactions on Industrial Electronics*, vol. 61, no. 5, pp. 2402–2411, 2014.

[5] X. Q. Fu, C. Wang, H. C. Yu, Y. G. Wang, and T. H. Wang, "Fast humidity sensors based on CeO_2 nanowires," *Nanotechnology*, vol. 18, no. 14, Article ID 145503, 2007.

[6] S. Yin, S. Ding, A. Haghani, H. Hao, and P. Zhang, "A comparison study of bacis data-driven fault diagnosis and process monitoring methods on the benchmark Tennessee Eastman process," *Journal of Process Control*, vol. 22, no. 9, pp. 1567–1581, 2012.

[7] Q. Kuang, C. Lao, Z. L. Wang, Z. Xie, and L. Zheng, "High-sensitivity humidity sensor based on a single SnO_2 nanowire," *Journal of the American Chemical Society*, vol. 129, no. 19, pp. 6070–6071, 2007.

[8] G. Garcia-Belmonte, V. Kytin, T. Dittrlch, and J. Bisquert, "Effect of humidity on the ac conductivity of nanoporous TiO_2," *Journal of Applied Physics*, vol. 94, no. 8, pp. 5261–5264, 2003.

[9] Y. Qiu and S. Yang, "ZnO nanotetrapods: controlled vapor-phase synthesis and application for humidity sensing," *Advanced Functional Materials*, vol. 17, no. 8, pp. 1345–1352, 2007.

[10] J. Wang and G. Song, "Mechanism analysis of $BaTiO_3$ and polymer QAR composite humidity sensor," *Thin Solid Films*, vol. 515, no. 24, pp. 8776–8779, 2007.

[11] E. B. Várhegyi, I. V. Perczel, J. Gerblinger, M. Fleischer, H. Meixner, and J. Giber, "Auger and SIMS study of segregation and corrosion behaviour of some semiconducting oxide gas-sensor materials," *Sensors and Actuators B*, vol. 19, no. 1–3, pp. 569–572, 1994.

[12] R. R. Piticescu, C. Monty, D. Taloi, A. Motoc, and S. Axinte, "Hydrothermal synthesis of zirconia nanomaterials," *Journal of the European Ceramic Society*, vol. 21, no. 10-11, pp. 2057–2060, 2001.

[13] D. K. Smith and B. A. Korgel, "The importance of the CTAB surfactant on the colloidal seed-mediated synthesis of gold nanorods," *Langmuir*, vol. 24, no. 3, pp. 644–649, 2008.

[14] H. Y. Jin, N. Wang, L. Xu, and S. Hou, "Synthesis and conductivity of cerium oxide nanoparticles," *Materials Letters*, vol. 64, no. 11, pp. 1254–1256, 2010.

[15] S. Yin, S. Ding, A. Haghani, and H. Hao, "Data-driven monitoring for stochastic systems and its application on batch process," *International Journal of Systems Science*, vol. 44, no. 7, pp. 1366–1376, 2013.

[16] S. Brunauer, P. H. Emmett, and E. Teller, "Adsorption of gases in multimolecular layers," *Journal of the American Chemical Society*, vol. 60, no. 2, pp. 309–319, 1938.

[17] Z. D. Dohcevic-Mitrovic, M. J. Šćepanović, M. U. Grujić-Brojčin et al., "The size and strain effects on the Raman spectra of $Ce_{1-x}Nd_xO_{2-\delta}$ ($0 < x < 0.25$) nanopowders," *Solid State Communications*, vol. 137, no. 7, pp. 387–390, 2006.

[18] S. Patil, S. Seal, Y. Guo, A. Schulte, and J. Norwood, "Role of trivalent La and Nd dopants in lattice distortion and oxygen vacancy generation in cerium oxide nanoparticles," *Applied Physics Letters*, vol. 88, no. 24, Article ID 243110, 2006.

[19] Z. Xu, S. He, L. He, R. Mu, G. Huang, and X. Cao, "Novel thermal barrier coatings based on $La_2(Zr_{0.7}Ce_{0.3})_2O_7$/8YSZ double-ceramic-layer systems deposited by electron beam physical

vapor deposition," *Journal of Alloys and Compounds*, vol. 509, no. 11, pp. 4273–4283, 2011.

[20] X. Zhao, X. Liu, S. Yin, and H. Li, "Improved results on stability of continuous-time switched positive linear systems," *Automatica*, 2013.

[21] W. M. Qu and W. Wlodarski, "A thin-film sensing element for ozone, humidity and temperature," *Sensors and Actuators B*, vol. 64, no. 1–3, pp. 42–48, 2000.

[22] X. Zhao, L. Zhang, P. Shi, and H. Karimi, "Robust control of continuous-time systems with state-dependent uncertainties and its application to electronic circuits," *IEEE Transactions on Industrial Electronics*, 2013.

[23] R. Schaub, P. Thostrup, N. Lopez et al., "Oxygen vacancies as active sites for water dissociation on rutile TiO_2 (110)," *Physical Review Letters*, vol. 87, no. 26, Article ID 266104, 4 pages, 2001.

[24] X. Zhao, L. Zhang, P. Shi, and M. Liu, "Stability of switched positive linear systems with average dwell time switching," *Automatica*, vol. 48, no. 6, pp. 1132–1137, 2012.

[25] X. Zhao, L. Zhang, P. Shi, and M. Liu, "Stability and stabilization of switched linear systems with mode-dependent average dwell time," *IEEE Transactions on Automatic Control*, vol. 57, no. 7, pp. 1809–1815, 2012.